ARTICLE NO. 79-0136R

Analyses of Pressure Oscillations in an Open Cavity

W. L. Hankey* and J. S. Shang†
Air Force Flight Dynamics Laboratory, Wright-Patterson Air Force Base, Ohio

Open cavities on aircraft exposed to high-speed flow, such as weapon bays, can give rise to intense self-induced pressure oscillations. The amplitude of these oscillations, under certain flight conditions, can cause structural damage. Substantial experimental and analytical efforts have investigated these pressure fluctuations, resulting in some understanding of the complex interaction of the external shear layer and cavity acoustical disturbances. However, no numerical computations have been obtained for the complete governing fluid mechanical equations. The purpose of this study is to obtain numerical solutions of the Navier-Stokes equations for an open cavity in order to provide a new tool for the analysis of this phenomenon.

Nomenclature

a = speed of sound
A = coefficient in pressure perturbation equation
c = complex propagation speed
C_p = specific heat at constant pressure
D = cavity depth
e = specific internal energy
E,F = vector fluxes
f = frequency of wave
k = c_1/U_∞, propagation velocity ratio
L = cavity length
m = mode number
M = Mach number
n = node number
p = pressure
$\dot{q}$ = heat transfer rate
R = gas constant
Re = Reynolds number
t = time
T = temperature
u,v = velocity components in Cartesian frame
U = vector of dependent variables
x,y = Cartesian coordinates
α = $2\pi\delta/\lambda$, dimensionless wave number
γ = ratio of specific heats
δ = shear layer thickness
λ = wavelength
μ = viscosity (molecular and eddy)
ρ = density
σ = normal stress
τ = viscous shear stress
ϕ = amplitude of perturbation velocity
ω = $2\pi f$ frequency

Subscripts

∞ = freestream condition
0 = stagnation condition
w = wall condition
r = real part
i = imaginary part
1 = forward-traveling wave
2 = rearward-traveling wave

Superscripts

$( )'$ = instantaneous perturbation variable
$\bar{( )}$ = vector

Presented as Paper 79-0136 at the AIAA 17th Aerospace Sciences Meeting, New Orleans, La., Jan. 15-17, 1979; submitted March 28, 1979; revision received Jan. 25, 1980. This paper is declared a work of the U.S. Government and therefore is in the public domain.

Index categories: Nonsteady Aerodynamics; Viscous Nonboundary-Layer Flows.

*Senior Scientist. Associate Fellow AIAA.

†Aerospace Engineer. Associate Fellow AIAA.

I. Background

As early as 1955, Krishnamurty[1] investigated flow-induced pressure oscillations in open cavities. Other investigators[2-9] have conducted extensive research in an attempt to understand the physical mechanisms. Heller and Bliss[3] used a water table to simulate supersonic airflow over open cavities. They found that the inherently unstable shear layer fluctuates, causing periodic mass addition and expulsion from the cavity (Fig. 1). When the rear reattachment point of the shear layer enters the cavity, a stagnation point is created, thus increasing the local cavity pressure. This mass addition creates a traveling pressure wave (as in a shock tube), which moves forward in the cavity (at supersonic speed relative to freestream), trailing an oblique shock in the freestream. When the traveling shock wave reflects from the forward bulkhead, a pressure doubling occurs in the cavity while disturbances in the external flow are not reflected, and thus a pressure jump across the shear layer deflects the shear layer. The reflected traveling shock wave in the cavity is now moving at subsonic speed relative to the freestream and, hence, generates no oblique shock wave in the freestream. As the cavity traveling shock wave approachs the rear bulkhead, the shear layer bulges outward, and mass is ejected out of the cavity. The entire process then repeats itself in a periodic fashion.

Thus, sufficient experience from such extensive measurements exists so that a qualitative description of the flow process can be obtained. However, a quantitative prediction method does not exist, which is the motivation for the present investigation.

To study self-induced pressure oscillations in an open cavity, an analytic study was first accomplished, followed by a numerical computation of the Navier-Stokes equations and a comparison with previous experimental investigations.

II. Analytical Study

Consider a system of traveling waves which produce the wave-diagram (x,t) shown in Fig. 2. A resonant situation arises when a forcing function excites the shear layer in the frequency range where amplification is possible. The disturbances will grow until a limit cycle is reached due to viscous dissipation. A standing wave exists in the cavity when both the upstream and downstream traveling waves are synchronized. This wave pattern of Fig. 2 may be approximated by considering forward and rearward traveling pressure waves of equal intensity but different propagation velocities and wave numbers.

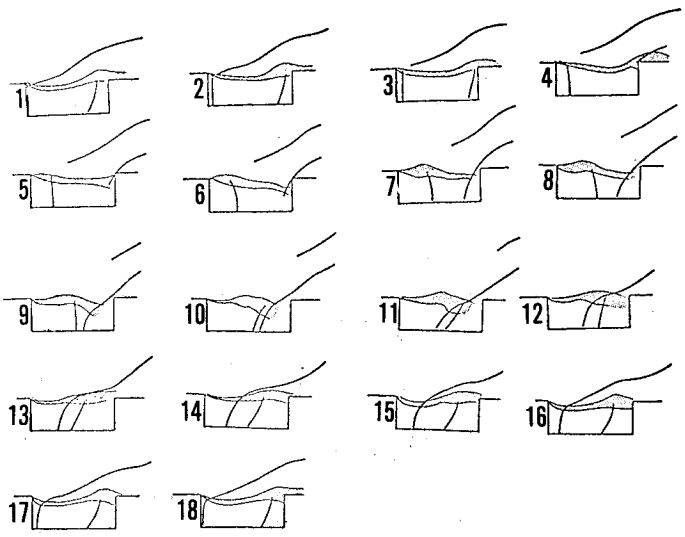

Fig. 1 Typical pressure oscillation cycle (Ref. 3).

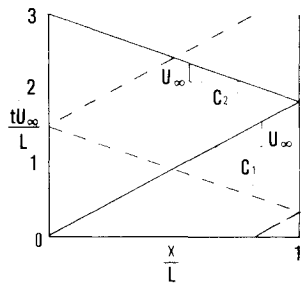

Fig. 2 Wave diagram.

$$p' = Ae^{i\alpha_1(x-c_1t)} + Ae^{i\alpha_2(-x-c_2t)} \tag{1}$$

The frequency of the pressure pulse can be determined directly from the wave-diagram.

$$m/f = (L/c_1) + (L/c_2) \tag{2}$$

where m is the number of waves or mode number.

From observation of cavity oscillations, the rearward traveling wave (α_2) is known to be an acoustical disturbance traveling at the speed of sound in the cavity.

$$c_2 = U_\infty \sqrt{1+0.2M_\infty^2}\; M_\infty^{-1} \tag{3}$$

The propagation speed of the forward traveling wave has been observed to be about half of the freestream value.[6]

$$c_1/U_\infty \equiv k \sim 1/2 \tag{4}$$

The frequency can be evaluated by using these results.

$$f = \frac{mU_\infty}{L(M_0 + k^{-1})} \text{ Rossiter's formula}^4 \tag{5}$$

This equation has been used successfully for determining cavity resonant frequencies, but no satisfactory prediction method has been available for determining the disturbance intensity of the different modes.

The mode shape of these standing waves can also be deduced from the preceding equations. For a standing wave to occur, both waves must possess the same frequency.

$$\omega = \alpha_1 c_1 = \alpha_2 c_2 = 2\pi f \tag{6}$$

Combining this result with Eq. (2) produces the following relationship:

$$\alpha_1 + \alpha_2 = 2\pi m/L \tag{7}$$

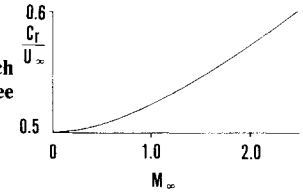

Fig. 3 Propagation velocity vs Mach number of traveling waves in a free shear layer (Ref. 12).

The mode shape may be obtained by utilizing this information in the pressure equation [Eq. (1)] and computing the rms value of pressure over a complete cycle.

$$p_{\text{rms}} = A(1+\cos(\alpha_1+\alpha_2)x)^{1/2}$$

$$p_{\text{rms}} = A\,|\cos m\pi x/L| \tag{8}$$

These patterns have been documented in Ref. 3. Nodes will occur when

$$m\pi x/L = n(\pi/2); \quad n = \text{odd}$$

and are displayed in Table 1.

III. Stability Analysis

A necessary condition for resonance is that one of the waves must be unstable for the oscillation to persist, otherwise the disturbance will dissipate after an initial transient. Mathematically, this means that the wave speed is complex, i.e., $c = c_r + ic_i$ with $c_i > 0$ unstable. The stability of the shear layer will now be examined.

In 1880, Rayleigh[10] showed that velocity profiles with inflection points are unstable for inviscid incompressible flow. Recently, Michalke[11] confirmed that a shear layer is unstable, but only at low frequencies ($\lambda/\delta > 2\pi$ or $f\delta 4\pi/U_\infty < 1$). It was felt that more information about the stability of a compressible shear layer was needed; therefore, a linear stability analysis was undertaken.[12] The governing Euler equations were linearized by assuming small perturbations caused by small amplitude traveling waves. The resulting stability equation first derived by Lees and Lin[13] reduces to the Rayleigh equation for incompressible flow.

$$a^2[g^{-1}(U-c)\phi_y - g^{-1}U_y\phi]_y = \alpha^2(U-c)\phi \tag{9}$$

where

$$v = \phi(y)e^{i\alpha(x-ct)} \tag{10}$$

$$g = a^2 - (U-c)^2 \tag{11}$$

The eigenvalues of this Rayleigh equation were then computed[12] for a shear layer with a hyperbolic tangent velocity profile.

$$U/U_\infty = 0.5[1+\tanh(y/\delta)] \tag{12}$$

The propagation velocity (c_r) of the disturbances is shown in Fig. 3.

$$c_r/U_\infty = k \tag{13}$$

Table 1 Node location for various modes

Mode m	Nodes n 1	3	5
1	1/2	—	—
2	1/4	3/4	—
3	1/6	3/6	5/6

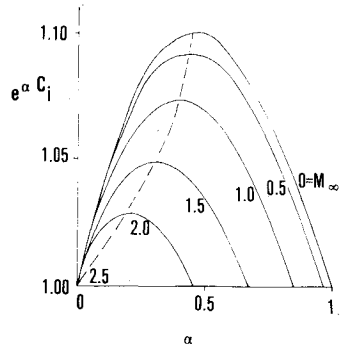

Fig. 4 Amplification factor vs wave number for different Mach number.[12]

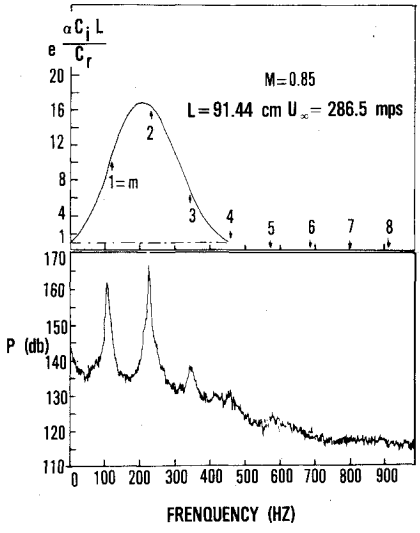

Fig. 5 Comparison of amplification for different frequencies with experimental data.

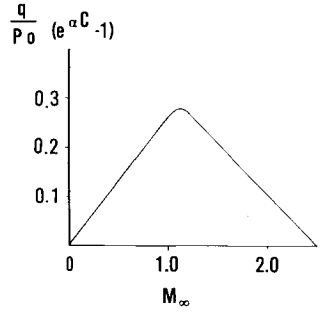

Fig. 6 Relative intensity of disturbances for different Mach numbers.

This is the k value determined experimentally by Rossiter[6] and found to be in excellent agreement with his results.

$$0.5 < k < 0.6$$

The amplification factors ($c_i > 0$) were found to be a function of wave number (α) and Mach number (Fig. 4). Instability was observed only for wave numbers less than unity. This implies short cavities ($L < 2\pi\delta$) will not resonate. Note that the Rayleigh instability vanishes above $M = 2.5$. This result confirms previous experimental and numerical results that separated flows and more stable at supersonic speeds than at subsonic.

It is possible to predict the relative intensity of the different modes occurring in an open cavity. Consider a cavity of $L = 91.44$ cm, $M_\infty = 0.85$, and $U_\infty = 286.5$ m/s.

Hence, $c_r/U_\infty = k = 0.52$ (from Fig. 3), $M_0 = 0.79$, and $f = 115$ Hz (Rossiter's equation).

These different mode frequencies are plotted in Fig. 5 using results of Ref. 12. The second mode is observed to have the greatest amplification, while modes four and above are found

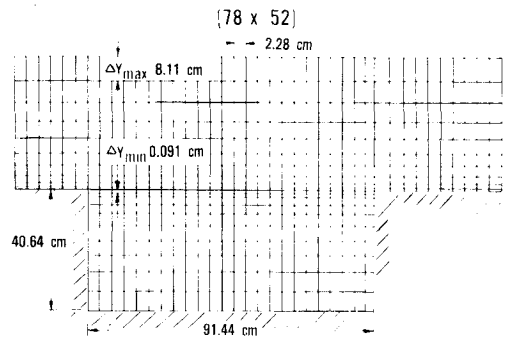

Fig. 7 Computational domain and mesh point distribution for numerical investigation.

to be stable. A spectral analysis of a wind tunnel test (Ref. 14) for an open cavity at these same conditions is also shown in Fig. 5. Observe that only the first four modes are dominant, and the relative amplitudes of these four modes are consistent with the analytic amplification factors.

The intensity of the pressure fluctuation will be proportional to the following:

$$p_{\text{rms}}(M) \sim q(e^{\alpha c_i} - 1) \tag{14}$$

By selecting the peak value of $e^{\alpha c_i}$ for each Mach number and multiplying the $q/P_0(M)$, the relative intensity as a function of Mach number may be deduced (Fig. 6). The peak pressure value occurring in a series of wind tunnel tests at different Mach numbers can be expected to occur near Mach one. This is confirmed in Refs. 3 and 14.

IV. Summary of Analytic Results

The analytic results based primarily upon stability theory provide us with the following conclusions:

1) Shear layers (with inflection points in the velocity profile) are unstable, but only for low frequencies; $f\delta/U_\infty < 1/4\pi$.

2) Short cavities ($L < 2\pi\delta$) will not resonate.

3) No Rayleigh instability occurs above Mach number 2.5.

4) Peak amplification occurs at about half the cut-off frequency, creating a situation where modes other than the fundamental can dominate.

5) Maximum pressure intensity of a shear layer oscillation will occur near Mach 1 (in a wind tunnel with constant p_0).

Liner stability theory is therefore useful in explaining the cause of the resonance and in estimating the relative intensity of the various modes including the influence of Mach number. However, the full nonlinear equations are required to determine the absolute level of the pressure intensity. For that reason, the numerical solution of the unsteady Navier-Stokes equations will be considered next.

V. Numerical Computation

With the completion of the simplified analytic approach (i.e., inviscid, linear stability theory), a numerical solution of the exact equations was attempted to further improve the prediction capability. The analysis served to identify the primary mechanism involved in the oscillation and greatly assisted in the determination of the grid point distribution and step sizes required to resolve the flow features.

A case to compute was selected for which experimental data were available. The test conditions of Heller and Bliss[3] were selected to compare the numerical computations (Fig. 7): $M = 1.5$, $L = 91.44$ cm, $L/D = 2.25$, $D = 40.64$ cm, $Re = 1.28 \times 10^6$/m, and $\delta_0 = 2.54$ cm.

The width of the cavity was 22.86 cm and found not to be a major factor in the overall phenomenon. For this reason, a two-dimensional computation appeared to be justified for the initial studies.

VI. Governing Equations

The time-dependent explicit finite difference method originated by MacCormack[15] was selected to perform the numerical calculations. The two-dimensional Navier-Stokes equations follow:

$$\frac{\partial U}{\partial t}+\frac{\partial E}{\partial x}+\frac{\partial F}{\partial y}=0 \tag{15}$$

$$U=\begin{vmatrix}\rho\\ \rho u\\ \rho v\\ \rho e\end{vmatrix};\quad E=\begin{vmatrix}\rho\\ \rho u^2-\sigma_{xx}\\ \rho uv-\tau_{xy}\\ \rho ue-u\sigma_{xx}-v\tau_{xy}-\dot{q}_x\end{vmatrix}$$

$$F=\begin{vmatrix}\rho v\\ \rho uv-\tau_{xy}\\ \rho v^2-\sigma_{yy}\\ \rho ve-v\sigma_{yy}-u\tau_{xy}-\dot{q}_y\end{vmatrix} \tag{16}$$

where

$$\sigma_{xx}=-p-2/3\mu\nabla\cdot\bar{u}+2\mu u_x$$

$$\tau_{xy}=\mu(u_y+v_x)$$

$$\sigma_{yy}=-p-2/3\mu\nabla\cdot\bar{u}+2\mu u_y \tag{17}$$

The turbulent closure of the present problem was achieved by implementing the Cebeci-Smith eddy viscosity model with relaxation modification.[16] The relaxation turbulence model was used in an attempt to describe the adjustment of the turbulence structure from an attached boundary layer to an oscillatory free shear layer. The relaxation length scale was assigned a value of 55 boundary-layer thicknesses. Since there is no guidance to assess the accuracy of the turbulence model relative to low-frequency fluctuations, a parametric study seemed to be necessary. In the present analysis, several consecutive calculations with suppressed eddy viscosity were performed, and the numerical results exhibited only a minor departure from the basic solution. Hence, the present eddy viscosity model was felt to be adequate. The computer program previously used by Shang[16,17] was modified to include the appropriate boundary conditions for this problem.

VII. Boundary Conditions

Four faces require attention in the specification of boundary conditions (Fig. 7).

Wall and Cavity Surfaces

On solid surfaces, the velocity components vanish, and the wall temperature must be prescribed. In addition, the pressure is derived from the respective compatibility conditions of the momentum equations.

$$u=0 \quad v=0 \quad T_w=T_0$$

$$\frac{\partial p}{\partial x}=\frac{\partial}{\partial x}[-2/3\mu\nabla\cdot u+2\mu u_x]-\frac{\partial}{\partial y}[\mu(u_y+v_x)]$$

$$\frac{\partial p}{\partial y}=\frac{\partial}{\partial y}[-2/3\mu\nabla\cdot u+2\mu u_y]-\frac{\partial}{\partial x}[\mu(u_y+v_x)] \tag{18}$$

Upstream Condition

A supersonic freestream with a known boundary-layer profile is given.

$$u=u(y),\quad T=T_0-(u^2/2C_p),\quad v=0,\quad p=p_\infty \tag{19}$$

Downstream Condition

A mild boundary condition is prescribed to avoid major reflections of disturbances.

$$\frac{\partial u}{\partial x}=0,\quad \frac{\partial T}{\partial x}=0,\quad \frac{\partial v}{\partial x}=0,\quad \frac{\partial p}{\partial x}=0 \tag{20}$$

Upper Boundary

A similar no-reflection condition is adopted.

$$\frac{\partial u}{\partial \zeta}=0,\quad \frac{\partial T}{\partial \zeta}=0,\quad \frac{\partial v}{\partial \zeta}=0,\quad \frac{\partial p}{\partial \zeta}=0 \tag{21}$$

where ζ are the outgoing characteristics on the upper boundary of the computational domain.

Initial Condition

The upstream condition is imposed as the initial condition for the flow outside the cavity. Inside the cavity, initially, the flow is assumed to be static.

$$u=0 \quad v=0 \quad T=T_0 \quad p=p_\infty \tag{22}$$

VIII. Numerical Procedure

MacCormack's[15] alternating-direction explicit numerical scheme was adopted for the present analysis. For this case, pressure damping was required due to the transient multiwave structure occurring in the flowfield. The current philosophy in computational fluid dynamics is to employ a body oriented coordinate system, which turns out to be Cartesian in this case with nonuniform step size. For cases presented here, a grid of 78×52 was used to represent a field size of 182.9×91.44 cm enclosing a 91.44×40.64-cm cavity (see Fig. 7). In order to achieve the desired temporal resolution, a time step corresponding to a Courant number of 0.2 was used. All calculations were performed on a CDC 6600 computer. The data processing rate was 0.0017 s per grid point per time step. The central core memory required for the present problem is 205K octal.

Although dispersion, dissipation, and phase errors are not negligible with the step sizes employed, previous numerical investigations of viscous interaction problems[15,16] using comparable step sizes have shown good agreement ($\pm5\%$) with experimental data for the most significant features of the flow. In particular, periodic motions around a transonic airfoil have been studied by Levy[18] with a basic MacCormack's scheme. His results exhibited good agreement with experimental data not only in the pattern of a simple wave train, but also in the predicted reduced frequency. Therefore, no additional modification other than a simple controlled spatial averaging was used to correct the possible dispersion error for the compound wave problem investigated.

IX. Discussion of Results

Time-dependent numerical computations of supersonic flow over an open cavity were accomplished utilizing MacCormack's finite difference explicit method. The entire velocity field over the cavity is shown in Fig. 8. Since the problem is strictly a time-dependent phenomenon, only a typical velocity distribution is presented here ($t=0.0062$ s) to reveal the basic features. The most obvious feature is that the flowfield within the confined cavity is subsonic, except perhaps the region adjacent to the cavity opening. The experimental investigation[3] also recorded the identical observation. The orderly development of the shear layer above the cavity is also clearly exhibited. An attached turbulent boundary layer upstream of the cavity separates at the forward bulkhead to form a free shear layer over the cavity and finally reattaches downstream of the cavity. Due to the

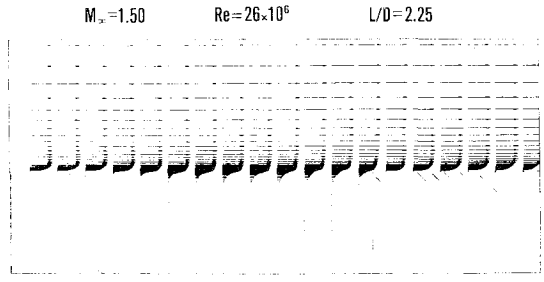

Fig. 8 Velocity of the entire flowfield ($t=3t_{ch}$). $M_\infty=1.50$, $Re=2.6\times10^7$, $L/D=2.25$.

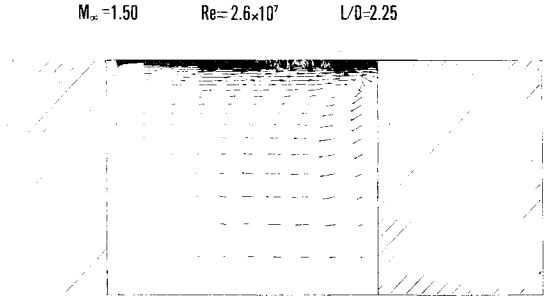

Fig. 9 Velocity profiles within the cavity ($t=t_{ch}$). $M_\infty=1.50$, $Re=2.6\times10^7$, $L/D=2.25$.

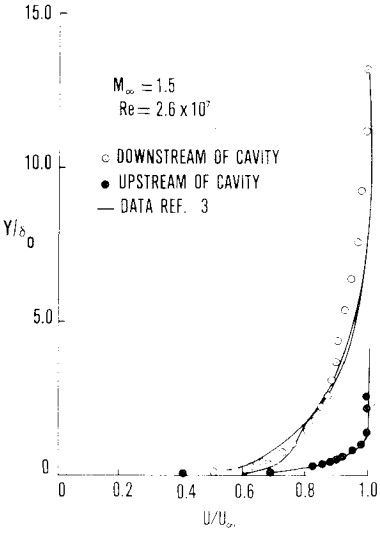

Fig. 10 Comparison of velocity profiles.

smaller magnitude of the velocity components within the cavity, the velocity distribution could not be shown with the same scale as that of the outer shear layer. A magnified velocity profile in the cavity is presented in Fig. 9. All velocity distributions were drawn at a scale ten times greater than that in Fig. 8. A recirculation flow configuration is demonstrated with the center of the recirculation located near the upper corner of the rear bulkhead. For clarity, only every fourth velocity point in the streamwise direction was presented in both Figs. 8 and 9.

A quantitative comparison of the calculated mean velocity distribution with experiment is presented in Fig. 10. The calculated velocity profile immediately upstream and downstream of the cavity compares very well with the experimental measurements. The upstream velocity profile is essentially independent of time, as expected, and nearly duplicates the data. The downstream velocity profile indicates that the reattached shear layer thickens significantly over the cavity. The difference between data and calculation is a mere 7%. The computed velocity profile downstream of the cavity

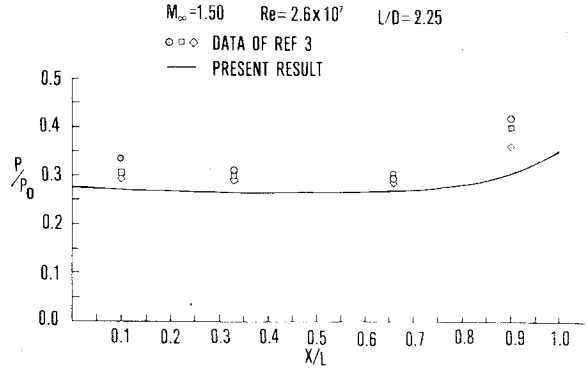

Fig. 11 Comparison of mean static pressure over the cavity.

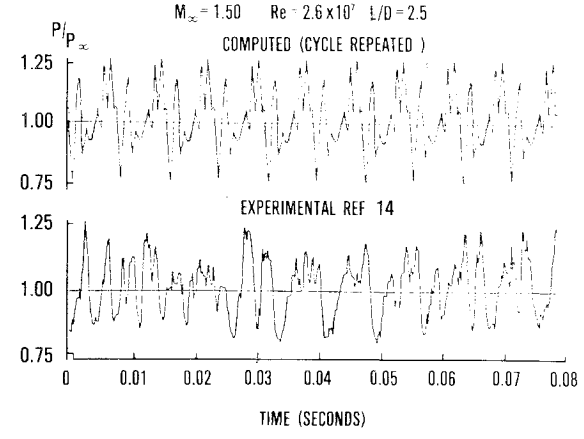

Fig. 12 Pressure history in the cavity.

exhibits an oscillatory behavior in the inner portion of the bounday layer which is confirmed by the experimental observation.

A comparison of the time-average surface pressure distribution in the cavity was performed. In Fig. 11, one observes that the computed mean pressure, normalized by the free stagnation pressure, uniformly underpredicts the experimental data[3] by about 10%. The maximum deviation between data and calculation occurs near the rear bulkhead where the pressure difference across the cavity opening and cavity floor also reaches a maximum. Nevertheless, the calculated results indicate the identical trend to that of the experiment.[3]

In Fig. 12, a history of the static pressure at $x/L=0.66$ and $y/L=0.960$ is monitored ($y/L=0.960$, $x/L=0.33$, 0.50, and 0.66). Persistent oscillatory static pressures appeared within one characteristic time t_{ch}. The characteristic time is defined as the period of time required for a fluid particle to traverse the length of the cavity at freestream speed. For the present problem, t_{ch} has a value of 1.987×10^{-3} s. Since the pressure oscillation over the cavity is composed of several frequencies of different amplitude, a compound wave system develops. The present calculation was carried out only over a time span of about nine characteristic times ($t=1.82\times10^{-2}$ s). This result is compared with oscillogram data for the test results of Ref. 18 in Fig. 12. In order to permit a qualitative comparison, computed results are repeated for several cycles. One can detect certain similarity between the data and the present result. In principle, the solid surface constraint and wave interference phenomenon of the present problem are inherently nonlinear. Therefore, caution must be exercised in discerning the discrete frequencies between the fundamental modes of oscillation. Other basic information such as the relative phase angle and the amplitude of each distinctive wave requires further spectral analysis.

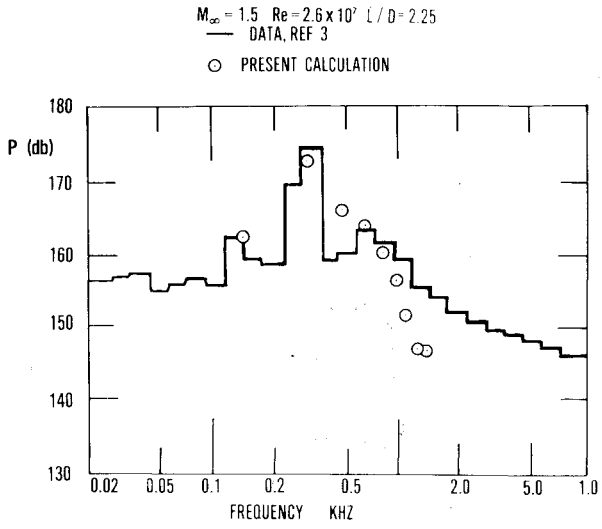

Fig. 13 Comparison of spectral analysis results.

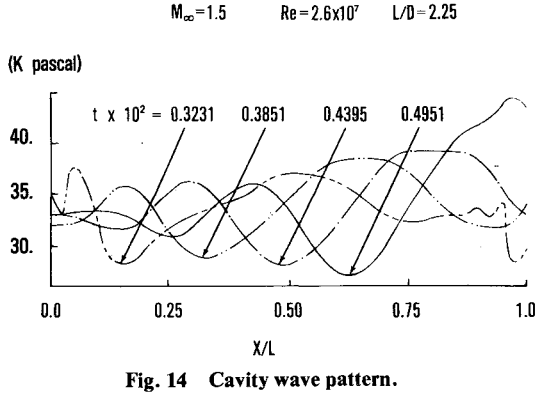

Fig. 14 Cavity wave pattern.

A spectral analysis of this compound wave probably is the only reliable means for accurately obtaining mode frequency. However, this is impractical due to the large amount of computer time required to obtain solutions for a sufficiently long duration. Hence, an analysis was accomplished by assuming the waves to be commensurable. The spectral analysis reveals four distinctive discrete frequencies of 154, 308, 462, and 616 Hz recognized as the first, second, third, and fourth mode, respectively, of the oscillatory pressure disturbance. The higher modes of oscillation decay rapidly, as one may observe in Fig. 13. Good agreement between the experimental measurement and present result is observed. Both exhibit a dominant second mode of the pressure oscillation. The level of pressure oscillation in dB can be evaluated as

$$p(\mathrm{dB}) = 20\log(p_{\mathrm{rms}}/q_\infty) + 189$$

where q_∞ is the dynamic pressure (54 kPa). The detected frequency for the second mode (308) compares well with the experimental data (300 Hz) and Rossiter's prediction[6] (328 Hz). The fluctuating pressure level between the data and present result is within about 10%.

The compound wave pattern is best illustrated in Fig. 14. The propagation of the wave train from the forward bulkhead is presented for a fixed time interval of 0.64×10^{-3} s. One observes that the rearward traveling propagation wave has an unmodulated amplitude until interacting with reflected waves from the rear bulkhead. No repeatable wave front can be identified downstream of $x/L = 0.75$. Two pieces of important information have been determined from this graph, namely the rearward wave propagation speed and the amplitude of

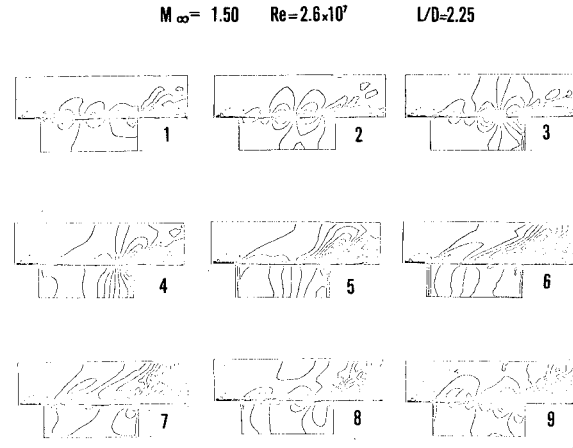

Fig. 15 Sequence of density contours. $M_\infty = 1.50$, $Re = 2.6\times10^7$, $L/D = 2.25$.

the pressure oscillation. The predicted wave speed has a value of 244.4 m/s (or $k = 0.53$) and is in agreement with the predicted value from Fig. 3. The amplitude of the oscillating pressure also agrees well with data (±6.464 kPa vs 7.182 kPa; or 170 dB) with the discrepancy about 10%.

In Fig. 15, the sequence of density contours from the numerical computation is shown for a complete cycle of the periodic motion. The forward and rearward moving wave system, originated from the instability of the free shear layer, and the reflection at the rear bulkhead can be easily recognized in the cavity. The generation and movement of the external shock wave system also can be recognized. These compare favorably with the wave pattern shown in Fig. 1 for the water table experiment.

X. Conclusions

The pressure oscillation for supersonic flow over an open cavity has been predicted by numerically solving the unsteady Navier-Stokes equations. Both the predicted frequency and magnitude of the unsteady pressure fluctuations were qualitatively confirmed through experiment. However, a spectral analysis of a numerical solution of longer duration is required for complete verification. This is the first time a complete viscous solution of the pressure oscillating cavity has been obtained, and it displays the outstanding capability inherent in the numerical methods of today.

References

[1] Krishnamurty, K., "Acoustic Radiation from Two-Dimensional Rectangular Cutouts in Aerodynamic Surfaces," NACA TN 3487, Aug. 1955.

[2] Heller, H., Holmes, G., and Covert, E., "Flow-Induced Pressure Oscillations in Shallow Cavities," Wright-Patterson Air Force Base, Ohio, AFFDL-TR-70-104, Dec. 1970.

[3] Heller, H. and Bliss, D., "Aerodynamically Induced Pressure Oscillations in Cavities: Physical Mechanisms and Suppression Concepts," Wright-Patterson Air Force Base, Ohio, AFFDL-TR-74-133, Feb. 1975.

[4] Clark, R. L., "Weapons Bay Turbulence Reduction Techniques," Wright-Patterson Air Force Base, Ohio, AFFDL-TM-75-147, Dec. 1975.

[5] Mainquist, R. S., "An Experimental Investigation into the Suppression of Flow-Induced Pressure Oscillations in Two-Dimensional Open Cavities," AFIT Thesis, March 1978.

[6] Rossiter, J. E., "Wind-Tunnel Experiment on the Flow over Rectangular Cavities at Subsonic and Transonic Speeds," British A.R.C.,R&M No. 3428, Oct. 1964.

[7] Spee, B. M., "Wind-Tunnel Experiments on Unsteady Cavity Flow at High-Subsonic Speeds," Separated Flow II, *AGARD Conference Proceedings*, Rhode-Saint-Genèse, Belgium, No. 4, May 1966.

[8] Quinn, B., "Flow in the Orifice of a Resonant Cavity," *AIAA Student Journal*, Vol. 1, April 1963.

[9] Borland, C. J., "Numerical Prediction of the Unsteady Flowfield in an Open Cavity," AIAA Paper 77-673, 1977.

[10] Rayleigh, Lord, "On the Stability or Instability of Certain Fluid Motion," *Scientific Papers*, Vol. 1, 1880, pp. 474-484.

[11] Michalke, A., "On the Inviscid Instability of the Hyperbolic-Tangent Velocity Profile," *Journal of Fluid Mechanics*, Vol. 19, Aug. 1964, pp. 543-556.

[12] Roscoe, D. and Hankey, W., "The Stability of a Compressible Free Shear Layer," AFWAL-TR-80-3016, Oct. 1979.

[13] Lees, L. and Lin, C. C., "Investigation of the Stability of the Laminar Boundary Layer in a Compressible Fluid," NACA TN 1115, Sept. 1946.

[14] Maurer, O., "Investigation and Reduction of Weapons Bay Pressure Oscillations Expected in the B-1 Aircraft," Wright-Patterson Air Force Base, Ohio, AFFDL-TM-74-101, Nov. 1974.

[15] MacCormack, R. W. and Baldwin, B. S., "A Numerical Method for Solving the Navier-Stokes Equations with Application to Shock Boundary-Layer Interactions," AIAA Paper 75-1, Pasadena, Calif., Jan. 1975.

[16] Shang, J. S. and Hankey, Jr., W. L., "Numerical Solutions for Supersonic Turbulent Flow over a Compression Ramp," *AIAA Journal*, Vol. 13, Oct. 1975, pp. 1368-1374.

[17] Shang, J. S. and Hankey, Jr., W. L., "Numerical Solution of the Navier-Stokes Equations for a Three-Dimensional Corner," *AIAA Journal*, Vol. 15, Nov. 1977, pp. 1575-1582.

[18] Levy, Jr., L. L., "Experimental and Computational Steady and Unsteady Transonic Flows about a Thick Airfoil," *AIAA Journal*, Vol. 16, June 1978, pp. 564-572.